The Canadian Mineralogist
Vol. 37, pp. 27-36 (1999)

UNUSUAL FORMS OF AMORPHOUS SILICA FROM SUBMARINE WARM SPRINGS, JUAN DE FUCA RIDGE, NORTHEASTERN PACIFIC OCEAN*

IAN R. JONASSON[1]

Geological Survey of Canada, 601 Booth Street, Ottawa, Ontario K1A 0E8

MICHAEL R. PERFIT[1]

Department of Geology, University of Florida, Gainesville, Florida 32611, U.S.A.

Abstract

Some unusual forms of amorphous silica were formed in ephemeral warm spring vents along the rift axis of north Cleft Segment, Juan de Fuca Ridge, located off the Oregon coast. They are associated with low mounds constructed by the settling of fine sulfide smoke (pyrite and sphalerite) and precipitation of silica within clumps of juvenile tube-worms that choked vent orifices. The brief period of hydrothermal activity recorded by these mounds is interpreted to be synchronous with incremental spreading events that generated megaplumes in the area in 1989–1990. The earliest forms of silica that cement smoke or soot particles, and comprise 60% of the mound material, consist of microspheroids and amorphous masses. Later forms are more exotic; nested radial sprays of transparent cylindrical needles of silica nucleated on thin layers of spheroids that coat euhedral grains of sulfide minerals. These forms occur only inside worm-tube molds fossilized within sulfide soot matrix materials. They appear to represent the last gasp of waning hydrothermal activity.

Keywords: silica, amorphous, cylindrical needles, hydrothermal vents, smoke, Juan de Fuca Ridge.

Sommaire

Nous décrivons certaines formes inusuelles de silice amorphe découvertes dans des évents éphémères à eau tiède le long de l'axe de la ride de Juan de Fuca, dans la partie nord du secteur dit de Cleft, non loin de la côte de l'Orégon. Ces formes sont associées aux amoncellements venant de l'accumulation de fumée de sulfures (pyrite et sphalérite) et de la précipitation de silice au sein d'amas d'annélides tubulaires juvénils qui ont étouffé les orifices des évents. La brève période d'activité hydrothermale mise en évidence par ces amoncellements serait synchrone avec des incréments d'extension qui ont généré les mégaplumes dans la région en 1989–1990. Les manifestations précoces de silice cimentent les particules de fumée ou de suie, et constituent 60% de l'amoncellement; il s'agit de microsphérules et de masses amorphes. Les formes plus tardives sont davantage exotiques; les amas radiés et enchevêtrés d'aiguilles transparentes et cylindriques de silice ont pris naissance sur de minces couches de sphérules qui recouvrent des cristaux idiomorphes de sulfures. Ces formes ne se trouvent qu'à l'intérieur des moules des annélides tubulaires, fossilisés au sein de la matrice faite d'une suie de sulfures. Elles représenteraient le stade ultime d'une activité hydrothermale en décroissance.

(Traduit par la Rédaction)

Mots-clés: silice, amorphe, aiguilles cylindriques, évents hydrothermaux, fumée, ride de Juan de Fuca.

Introduction

Since the discovery of hydrothermal mineral deposits on the deep seafloor in the late seventies, many new and uncommon minerals have been described. Some are metastable and transient forms of more common minerals that likely would not survive protracted hydrothermal zone-refining of the deposits, seafloor weathering and burial diagenesis. All such minerals are of considerable interest to mineral deposit geologists because they provide clues to primary mechanisms of ore genesis that are unavailable in the geological records of ancient deposits. Among the more notable new minerals described on the deep seafloor are isocubanite (Caye

[1] *E-mail addresses*: ijonasso@nrcan.gc.ca, perfit@geology.ufl.edu
* Geological Survey of Canada contribution number 1998185.

et al. 1988), caminite (Haymon & Kastner 1986), gordaite (Nasdala *et al.* 1998), the copper analogue of pyrite, *i.e.*, CuS_2 (Oudin *et al.* 1990, I.R. Jonasson, unpubl. data, Galapagos Ridge) as well as a wide variety of native metals and intermetallic compounds (*e.g.*, Davydov *et al.* 1998). In weathered (gossanous) deposits of massive sulfides, hydrous sulfates and chlorides abound. For example, atacamite and its rarer polymorphs, botallackite and paratacamite, have been widely reported (*e.g.*, Embley *et al.* 1988, Hannington 1993), as well as sulfates, chlorides and chloride–sulfates of Zn, Cu, Co and Fe (*e.g.*, Oudin, 1983; Embley *et al.* 1988, I.R. Jonasson, unpubl. data, Axial Seamount). Uncommon sulfides such as kermesite, jalpaite, geocronite and realgar polymorphs appear to be plentiful in backarc massive sulfide deposits (Halbach *et al.* 1988). The rare mineral alacranite has been identified recently in submarine gold-bearing sulfides from a small volcano near Lihir Island, Papua – New Guinea (J. Percival, Geological Survey of Canada, pers. commun., 1998). All these minerals, and the more common sulfides of Cu, Zn and Fe, owe their existence to the fact that metal-laden debouching hydrothermal fluids of 200°–400°C are quenched in minutes by mixing with 2°C ambient bottom seawater, and precipitate their dissolved loads. This may take place within growing sulfide chimneys or in buoyant smoke-plumes above them.

A common gangue component of hydrothermal sulfide chimneys is translucent silica, which is found as gelatinous, amorphous aggregates and cements, amorphous, porous globular chains and spheroids, as well as bacterial or mould-cored filamentous webs (*e.g.*, Oudin 1983, Herzig *et al.* 1988, Juniper & Fouquet 1988, Hannington & Scott 1988, Pracejus & Halbach 1996). Low-temperature deposits of ferruginous, manganiferous or baritic amorphous silica (or opaline silica forms) have also been described as primary mounds or chimneys (*e.g.*, Stüben *et al.* 1994, Hannington & Jonasson 1992, Iizasa *et al.* 1998). Occurrences of microcrystalline silica (cristobalite, opal-*ct*) in submarine hydrothermal deposits are relatively rare (Halbach *et al.* 1988, Vanko *et al.* 1991, Urabe & Kusakabe 1990). Embley *et al.* (1988) described α-cristobalite from stockwork veinlets of chalcopyrite and pyrite in chloritized basalt from the 85.5°W sulfide mounds of East Galapagos Ridge. Acicular and fibrous forms observed there are very similar to synthetic cristobalite described by Flörke *et al.* (1990). Primary quartz is an insignificant mineral in modern surficial seafloor sulfide deposits (*e.g.*, Vanko *et al.* 1991); however, it is a common component of long-lived systems such as the TAG field, Mid-Atlantic Ridge, where chalcedony has been recrystallized (ODP, 1995).

In this study, we describe some unusual transparent, cylindrical needles of amorphous silica found in low mounds of sulfide soot that plugs vents of warm springs peripheral to high-temperature black smoker vent complexes. To the authors' best knowledge, these forms have not been described previously.

Location

Samples (ALV2260–3A2) were collected by the submersible ALVIN within an area of low-temperature venting, from the walls of a fissure that forms part of the spreading axis of north Cleft Segment, Juan de Fuca Ridge (Fig. 1A) at latitude 44°59.0'N, longitude 130°13.2'W at a depth of approximately 2250 m. In this area, the ridge crest is marked by a parallel array of eastward-facing stepped fissures (020°N) occupied at intervals by high-temperature black smoker chimneys (Koski *et al.* 1994).

The study area lies between Monolith and Fountain hydrothermal vents, about 100 m north of Monolith and about 30 m west of the main rift system (Fig. 1B). Location is probably accurate to within 20 m, given the uncertainties of seafloor navigation. The warm vents likely lie within the distal part of Monolith's hydrothermal influence. This zone of Cleft Segment saw a rejuvenation of intense hydrothermal activity in 1986 and, to a lesser extent, in 1989, as indicated by the generation of megaplumes (Baker 1994, Butterfield & Massoth 1994) likely as a result of incremental spreading events accompanied by dyke injection and lava eruption along the central rift line (Lowell & Germanovich 1995, Delaney *et al.* 1998). Monolith chimney itself was subjected to renewed growth on an older oxidized sulfide base. There, vigorous high-temperature venting is focused at the center of a broad, diffuse field of warm springs, associated with parallel fissures and collapse pits. The study area occupies an outer zone of this system (Embley & Chadwick 1994, Koski *et al.* 1994, Rona *et al.* 1997).

Field observations of smectite-coated rock surfaces on fractures, shimmering warm water, bacterial matte, and dead but largely intact worm-tubes indicate that rejuvenation of the diffuse vent fields had been short-lived, and that the study site had recently been much more active than at the time of sampling in July 1990. Submersible-guided video traverses in the immediate vicinity led to the discovery of several fresh but small inactive sulfide spires in line with the fissures. The sample site consists of a short, narrow gja whose vertical walls step down a few meters eastward. Pillow lava (mid-ocean basalts) flows are sheared, and their debris forms short piles of talus within the fissure; white bacterial mattes cover the talus and adjacent east-facing walls. Hard, glassy surfaces of the basalt talus are sooty where close to a 0.5 m hole that was slowly venting clear warm water at about 5°C.

Sample Descriptions

General description

Small chip samples (*ca.* 150 g) gouged from the wall and low (<0.5 m) mounds around the vent consist of green, glassy, perlitic, vesicular material initially mistaken for mid-ocean andesitic glass; however, closer

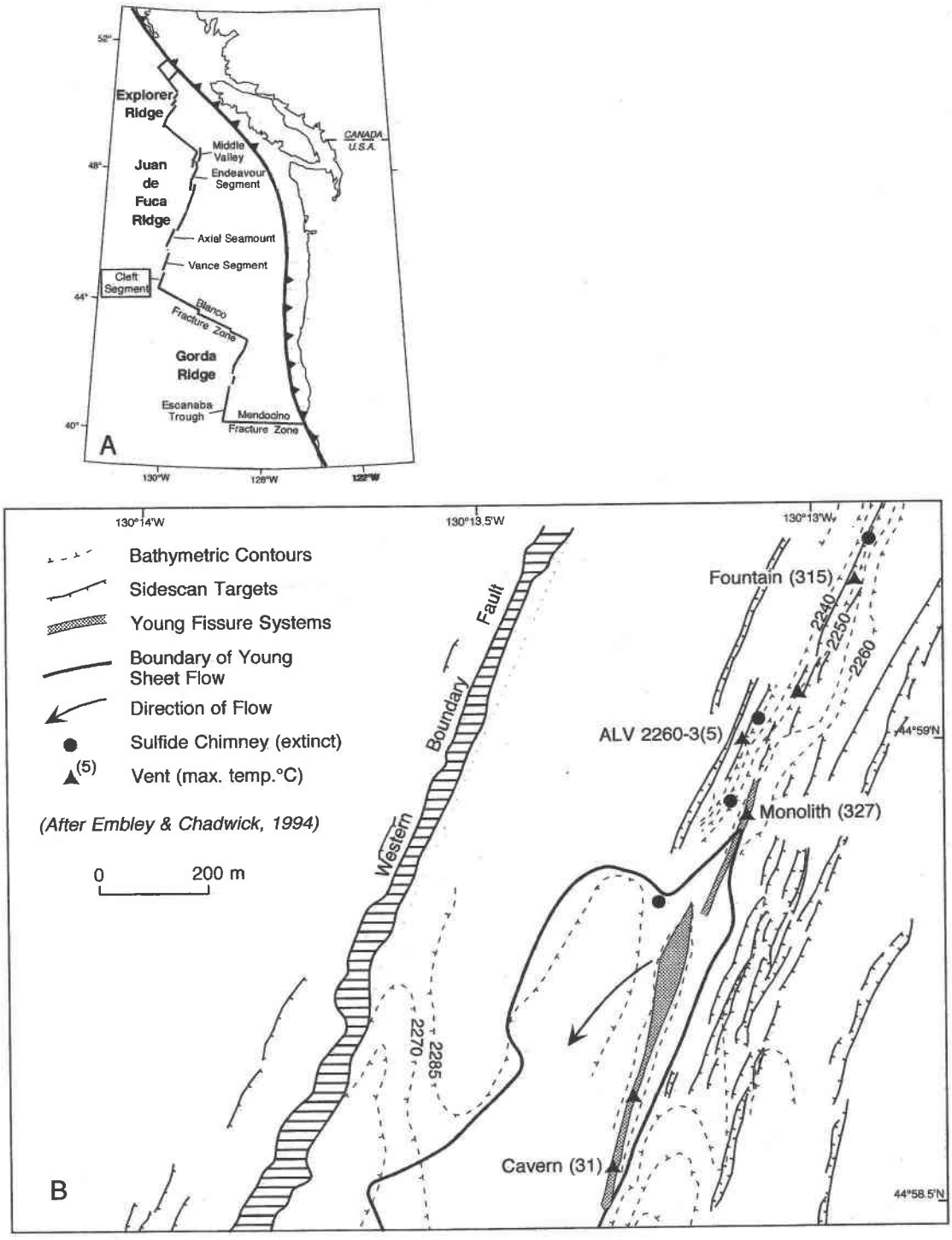

FIG. 1. A. Location of Cleft Segment of Juan de Fuca Ridge. B. Location and structural map of study site, ALV2260–3, between Monolith and Fountain black smoker vents. "Side scan targets" proved to be fissures when investigated by submersible deployment.

inspection showed the rocks to be aggregates of soot-like, fine-grained, granular sulfide particles well cemented by silica. Visual estimates suggested compositions of about 30 vol.% sulfides, with the remainder being silica. Subsequent examination with a binocular microscope revealed that the prominent circular vesicle-like cavities (up to 2 mm diameter) are lined with large (*ca.* 200 to 500 μm) columnar hexagonal crystals of intergrown sphalerite–wurtzite (identified by XRD), transparent spheroidal silica anchoring radiating sprays of transparent cylindrical needles (Figs. 2A, B). Minor sulfides present include chalcopyrite, isocubanite and pyrite. The cavities themselves were identified as closely spaced fossil worm-tubes from their orientation, shapes, and morphologies of their silicified walls (Figs. 3A, B, 4A).

Sphalerite particles occupy the siliceous matrix as porous, agglomerated irregular anhedral grains, and are closely intergrown with fine-grained filamentous pyrite and larger subhedra of pyrite. The grain size of sphalerite varies from a few micrometers up to about 500 μm. The larger, more porous grains are commonly blotchy (reflected light) and in part botryoidal. They are typically cored by and shaped around submicrometric to micrometric branching chains, or clumps of carbonaceous matter interpreted to be pyrolyzed remnants of bacterial matte (Figs. 4C, D). Pyrite takes similar forms (Fig. 4F), and also occurs less commonly as clusters of small (≤10 μm) porous framboids, or radial spheroids enclosing and infilling black annular rings of carbonaceous matter; all are embedded in irregular subhedral masses of brighter-reflecting pyrite. The larger, more euhedral grains of both sphalerite and pyrite are usually observed within small vugs in the siliceous matrix (Fig. 4C). Carbonaceous matter is largely preserved in the matrix silica, rather than in sulfides, and preferentially concentrated around in-filled voids.

Silica component

Silica assumes three forms in the samples: abundant, hard, near-featureless translucent to opaque matrix cement, minor transparent spheroids that line small, irregular vugs within matrix cement and encrust euhedral sulfides in worm-tubes, and rare cylindrical transparent needles that occur only in worm-tube molds (Figs. 2 to 4). All forms are X-ray-amorphous. Matrix silica is largely massive (Figs. 3B, 4A) but shows some relict textural evidence that it originated as coalesced spheroids (Figs. 4C, D). These are also present in worm-tube molds, typically as thin crusts on sulfides and underpinning sprays of silica needles (Figs. 2F, 3C, D) that form radiating clusters, interlocking and irregular nets, and may be intergrown or branching. Needles form colorless, transparent and smooth elongate cylinders terminating in hemispheres. They range in diameter from 10 to 60 μm, with highly variable length-to-diameter aspect ratios. However within a specific cavity and cluster, the diameter of each needle is constant, and the length, nearly so (Figs. 2A to F, 3A, E, 4B). About 20 molds were examined in support of these observations. SEM–EDS study and electron-microprobe analyses of matrix silica, spheroids and needles attest to the high purity of the silica. Analytical totals for all forms ranged between 97.4 and 99.6%; no trace components were detected. Electron-microprobe totals for needles (range 97.5–99.5%) averaged 98.7% (n = 6). Microdeterminations of H_2O are not available. Detailed examination of grain mounts and polished thin sections with a scanning electron microscope showed the needles to be largely solid, with no apparent channelways. However, a few rare clusters provide a clue to their mode of growth (Figs. 3E, F). These contain a core (1 to 10 μm), near-rhombic in shape, that may have formed capillary channels for silica-saturated hydrothermal fluid. Quantitative SEM–EDS analyses show that some of these conduits are infilled with an aluminosilicate bearing minor K and Ca (SiO_2 = 69.9%, Al_2O_3 = 11.6%, CaO + K_2O = 0.9%), but most were likely plugged by more silica and are no longer discernible by SEM back-scattered electron imagery. The rhombic to trapezoidal cross-sections are unexpected for channelways developed in X-ray amorphous silica.

Sulfides component

Sulfides are present in both siliceous matrix and enclosed worm-tube molds. Bulk analysis of chip samples (Table 1) confirms initial visual estimations of about two-thirds silica and one-third sulfides. Of the latter, only pyrite–marcasite (28 wt.%) and sphalerite–wurtzite (6 wt.%) are significant; chalcopyrite–isocubanite grains are rarely present, and moreover are confined to worm-

TABLE 1. WHOLE-ROCK COMPOSITIONS OF CHIP SAMPLES OF SILICIFIED SULFIDE SOOT MOUNDS, JUAN DE FUCA RIDGE

	(1)	(2)	(3)		(1)	(2)	(3)
SiO_2	63.4	65.1	66.3	Pb	405	325	500
TiO_2	<0.02	<0.02	<0.02	Ag	6	9	9
Al_2O_3	1.14	0.96	1.20	Co	250	198	182
Fe	13.51	13.01	12.30	Cr	11	12	10
MnO	0.02	0.02	0.02	Cu	310	170	210
MgO	<0.04	<0.04	<0.04	Ba	≤30	≤30	≤30
CaO	0.27	0.28	0.35	As	120	102	120
Na_2O	0.35	0.23	0.41	Sb	3.7	4.5	4.3
K_2O	0.12	0.19	0.14	Se	2.0	7.8	4.6
P_2O_5	0.08	0.10	0.06				
Zn	2.0	2.0	4.4				
S total	16.8	15.0	13.7				
Total	99.7	97.0	99.0				

Major elements (wt. %): ICP-ES; Trace elements (ppm): ICP-MS and flameless AAS. Elements sought but not detected (<5 ppm) include Be, La, Sc, Sr, Y, Zr. The levels of C org and H_2O were not determined. Visual estimates from thin sections indicate 1–2 vol.% carbonaceous matter.

tube molds (Figs. 4A, B). In the matrix soot, early-formed sphalerite (cream-reflecting) contains low Fe (av. 8.55 wt.%), Cd, As, but elevated Cu values, whereas late-generation sphalerite (grey-reflecting) that overgrows the former, carries elevated levels of Fe (av. 12.8 wt.%), Cd and As, but no detectable Cu (Fig. 4C). Small vugs in the sooty matrix are filled with subhedral to botryoidal (blotchy-reflecting) sphalerite typically overgrowing porous filamentous sphalerite, and late-stage spheroidal silica. The contents of iron and other trace elements fall into the same ranges of values as for matrix soot sphalerite. Data are summarized in Table 2 for the vug illustrated in Figures 4C and 4D. Early dendritic or filamentous pyrite has elevated levels of Zn (av. 0.32 wt.%), plus a little Cd and As; later-stage euhedral to subhedral pyrite is notable only for increased Ni and As contents. These data are summarized in Table 2, and paragenetic relationships are illustrated in Figure 4F.

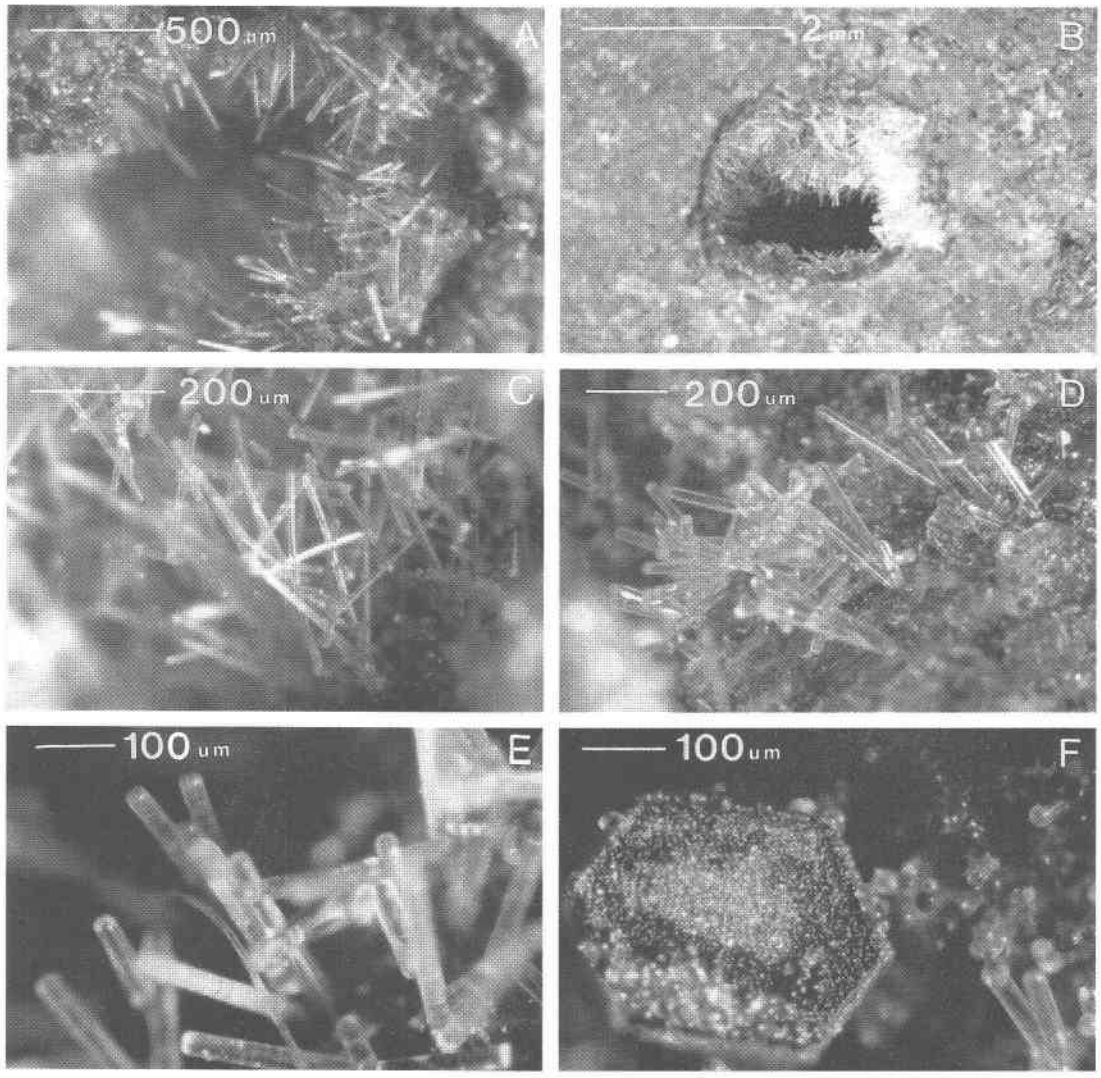

FIG. 2. Binocular photomicrographs of silica needles. A,B. Views of two worm-tube molds (2.5 mm) occupied by a rim of wurtzite–sphalerite crust overgrown by sprays and clusters of transparent needles of amorphous silica (10 µm diameter). Needles are cylindrical and terminate in hemispheres. C. Silica needles (10 µm diameter, 300 µm length) also form irregular nets of branching and intergrown arrays. D. Radial sprays of needles (25 µm diameter) nucleating on silica-covered wurtzite euhedra. E. Interlocking needles (30 µm diameter) in a worm-tube mold. F. Thin platelet of wurtzite coated in clear spheroidal silica, which typically forms the substrate to clusters of silica needles.

TABLE 2. RESULTS OF ELECTRON-MICROBEAM ANALYSES OF SULFIDES

	Av. Values (wt. %) Electron Microprobe							n.d. = not detected			
MATRIX SOOT	Zn	Fe	S	Cd	Ni	Cu	Co	Se	As	Mn	Total
Sphalerite	56.50	9.05	32.65	0.05	0.02	0.09	0.02	n.d.	n.d.	0.03	98.41
cream reflecting	55.77	9.95	32.99	0.13	0.01	n.d.	0.01	n.d.	0.02	0.05	98.93
early stage	57.65	8.32	33.01	0.05	n.d.	n.d.	0.01	n.d.	0.05	0.02	99.12
subhedral	57.56	10.04	30.50	0.07	0.04	0.01	0.03	n.d.	0.12	0.01	98.37
	60.35	5.39	31.96	0.06	0.01	0.29	n.d.	n.d.	0.01	0.04	98.11
Sphalerite	51.48	13.08	32.98	0.04	0.02	n.d.	0.02	n.d.	0.12	0.07	97.86
grey reflecting	55.18	12.03	33.50	0.21	0.02	n.d.	0.04	n.d.	0.04	0.03	101.04
late stage	52.75	13.23	33.33	0.18	0.05	n.d.	0.04	n.d.	0.07	0.04	99.68
botryoidal											
Pyrite	0.15	46.98	53.71	0.04	0.01	n.d.	0.05	0.06	0.12	n.d.	101.13
filamentous	0.49	46.84	53.48	0.09	0.01	n.d.	0.02	n.d.	0.07	0.02	101.02
early stage											
Pyrite	0.09	46.96	53.26	n.d.	0.05	n.d.	0.03	n.d.	0.08	0.02	100.48
subhedral	0.07	47.39	53.61	0.04	0.02	n.d.	0.06	0.01	0.08	0.05	101.33
late stage											
MATRIX VUGS	Av. Values (wt. %) Quantitative SEM-EDS										
Sphalerite	51.90	14.28	33.95	0.32	n.d.	n.d.	n.d.	n.d.	n.d.	n.d.	100.45
filamentous	52.15	11.54	33.29	0.31	0.15	n.d.	n.d.	n.d.	n.d.	n.d.	97.65
anhedral	54.40	11.55	33.89	0.32	n.d.	0.23	n.d.	n.d.	n.d.	n.d.	100.39
Sphalerite	55.56	11.16	33.68	n.d.	n.d.	n.d.	n.d.	n.d.	n.d.	n.d.	100.40
blotchy	55.60	10.57	33.80	n.d.	n.d.	n.d.	n.d.	n.d.	n.d.	n.d.	100.19
subhedral	57.08	10.12	33.99	n.d.	n.d.	n.d.	n.d.	n.d.	n.d.	n.d.	101.19
WORM-TUBE MOLDS	Av. Values (wt. %) Quantitative SEM-EDS										
Sphalerite	48.71	16.26	33.60	0.40	0.14	n.d.	n.d.	n.d.	n.d.	n.d.	99.11
euhedral	50.13	15.95	33.45	0.30	n.d.	n.d.	n.d.	n.d.	n.d.	0.13	99.96
basal layer											
Sphalerite	55.98	9.86	33.28	n.d.	n.d.	n.d.	n.d.	n.d.	n.d.	n.d.	99.12
anhedral											
top layer											
Sphalerite-Wurtzite	54.40	11.55	33.89	n.d.	n.d.	n.d.	n.d.	n.d.	n.d.	n.d.	100.4
hexag. prism											
Chalcopyrite	0.57	31.28	34.55	n.d.	n.d.	32.39	n.d.	n.d.	n.d.	n.d.	98.79
euhedral: core	0.61	31.51	34.32	n.d.	n.d.	32.16	n.d.	n.d.	n.d.	n.d.	98.60
euhedral: rim	0.47	30.92	34.47	n.d.	n.d.	33.50	n.d.	n.d.	n.d.	n.d.	99.36
	0.00	31.48	34.61	n.d.	n.d.	33.17	n.d.	n.d.	n.d.	n.d.	99.26
Pyrite	n.d.	46.34	53.38	n.d.	n.d.	n.d.	n.d.	n.d.	n.d.	n.d.	99.72
euhedral	n.d.	47.35	53.96	n.d.	n.d.	n.d.	n.d.	n.d.	n.d.	n.d.	101.31

In the worm-tube molds, a similar sequence of sulfide precipitation is apparent. Walls of cavities are lined by two distinctive layers of sphalerite, the earlier being Fe-rich (av. 16.1 wt.%), and the overlying layer, Fe-poor (9.86 wt.%). The Fe-poor layer consists of intergrown euhedral sphalerite and scattered overgrowths of more coarse-grained sphalerite–wurtzite as hexagonal prisms (XRD analysis), less common chalcopyrite ± isocubanite euhedra, and much rarer cubes of pyrite. Chalcopyrite zonation is due to the decrease in zinc content and increase in copper content from core to rim (Table 2). All euhedral sulfides are overgrown by the silica spheroids, and silica cylinders of unusual habit, already described (Figs. 3B, C, 4A, B). The composition of cavity sulfides is summarized in Table 2.

Discussion

Origin of the mounds

The samples analyzed are considered to be representative of sulfide smoke or soot mounds that precipitated

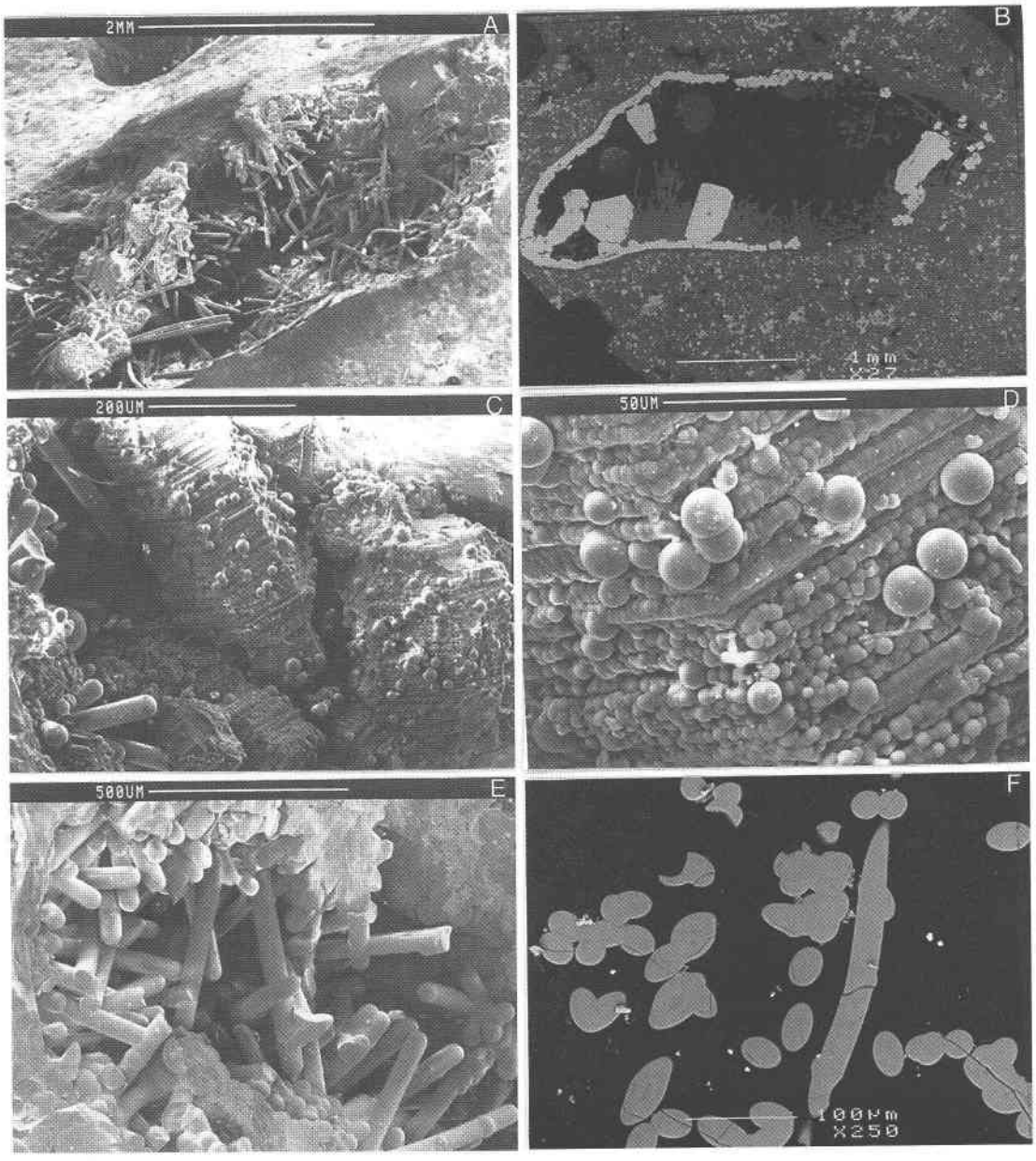

FIG. 3. SEM images of silica needles. A. Long section through a worm-tube mold showing a lining of silica-encrusted hexagonal prisms of wurtzite–sphalerite and rarer cubes of pyrite, from which silica needles radiate. Note some bent and branching varieties. All are 30 µm diameter (secondary electron image). B. Cross-section of worm-tube mold (thin section) displays a matrix of anhedral grains and clumps of pyrite and sphalerite embedded in porous amorphous silica. Tube walls are replaced by silica (darker grey) and lined by layered zinc sulfides. Large crystals are wurtzite (hexagonal) and chalcopyrite (rectangular). Sulfides are overgrown by spheroidal silica and nests of cylindrical needles of silica (dark grey) (back-scattered electron images). C. Hexagonal pillars of wurtzite showing strong basal cleavage are completely enveloped in spheroidal silica (secondary electron image; *cf.* Fig. 2A). D. Close-up detail of C; spheres are 2 to 15 µm diameter. E. Interior of a small (1 mm) worm-tube mold showing radiating and branching habits of cylindrical needles of silica. Note the constancy of needle diameter (30 µm). Lower right corner displays mode of nucleation and elongate radial growth of needles from spheroids (secondary electron image). F. Cluster of needles in cross-section: rare examples of needles with small trapezoidal cores (1 to 10 µm) through which silica-saturated fluids may have passed. Cavities are now filled with an aluminosilicate bearing minor K and Ca (back-scattered electron image).

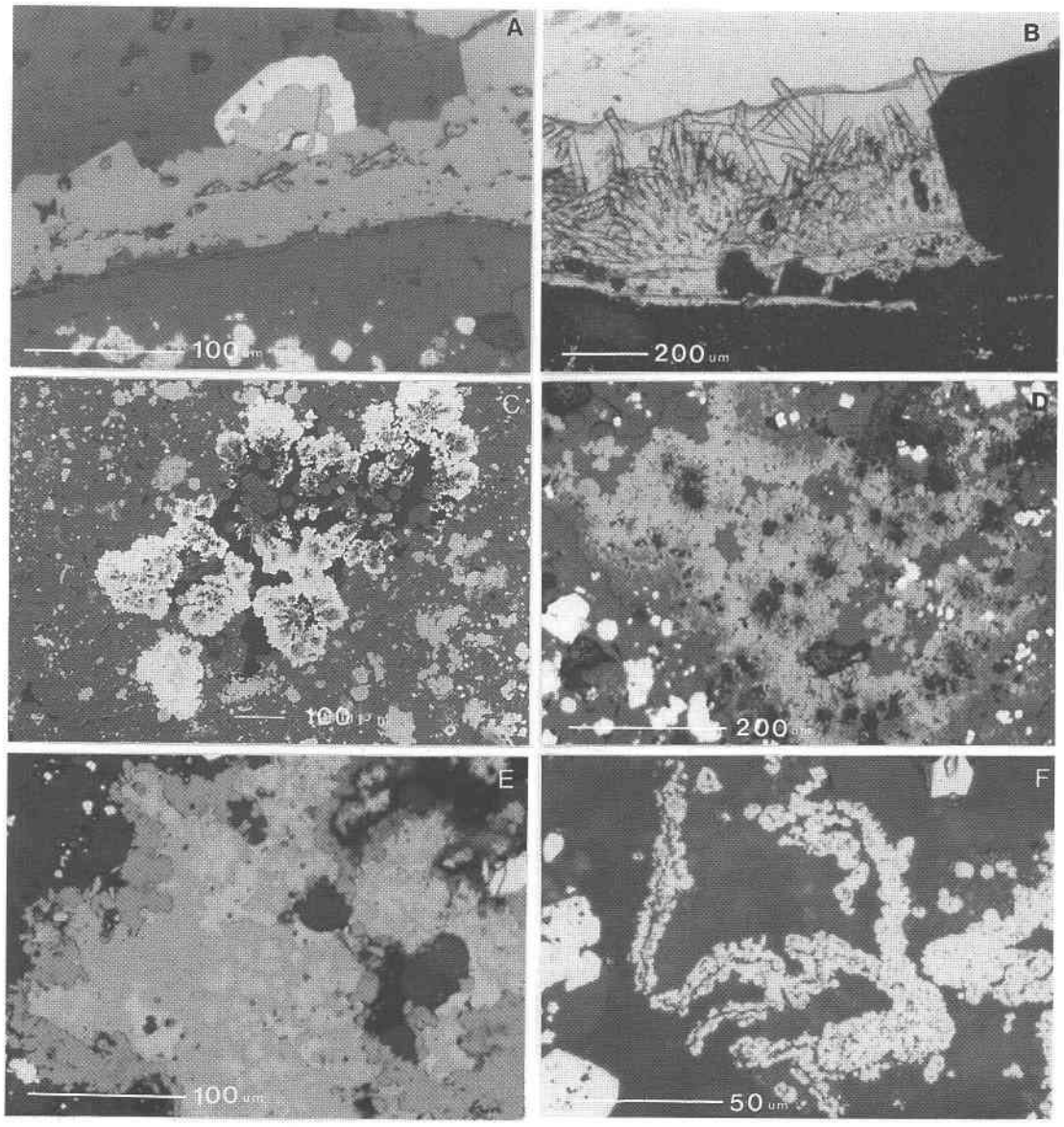

FIG. 4. Optical microscopy of sulfides. A. Cross-section of worm-tube wall shows, from the bottom to top: matrix pyrite, sphalerite in silica (grey); worm wall replaced by silica (darker grey) with a thin (5 μm) inner lining of spheroidal silica (darkest grey); two layers of zinc sulfides where Fe content decreases inward; large crystals of Fe-rich wurtzite plus chalcopyrite (bright zoned grain). Reflected light; *cf.* Figure 3B. B. Same void showing late silica needles overgrowing euhedral sulfide grains and partly infilling worm-tube mold (transmitted light). C. A partly infilled vug in sulfide–silica matrix lined by botryoidal sphalerite (bright) nucleated on branching clumps of bacterial matte (black). Note abundance of matte around open fluid channelway and spheroidal silica (grey) infill. Matrix sulfides are largely pyrite with enclosed carbonaceous matter (reflected light). D. Close-up detail of a similar void in matrix highlights the abundance and morphology of carbonized bacterial matte (black) enclosed in Fe-rich sphalerite (bright) and in void space. Sooty matrix consists of non-porous subhedral pyrite (brightest) and amorphous silica (grey) (reflected light). E. Large composite grains (~0.5 mm) of soot sphalerite of different hues (reflected light) related to Fe content. Earlier cream-colored forms (pale) are low in Fe, whereas later brown to grey forms (darker grey) contain more Fe. F. Much of the "smoke" sulfide matrix consists of small pyritized bacterial strings and fluff enveloped in amorphous silica (grey). Later sphalerite and subhedral pyrite overgrow and replace them (*cf.* Fig. 4C; reflected light).

and settled within the orifices of warm-water vents, by infilling and overgrowing small but dense clumps of juvenile upright worm-tubes and voluminous attendant bacterial floc that adhered to them. The organisms continued to flourish and grow until they were gradually inundated by adhering pyritic smoke particles as the clumps were infilled and low (a few to tens of cm) mounds formed. Flow-through of fluid was increasingly restricted as more sulfides were precipitated and sealed the system. This allowed subsurface temperatures to rise as ingress of cold seawater largely ceased. Warmer undiluted hydrothermal fluids, now able to transport more metal ions, precipitated sphalerite with increasing Fe contents in remaining channelways as temperatures continued to rise. Finally, they reached levels likely in the range 250–300°C (Koski *et al.* 1994) and precipitated complex intergrowths of sphalerite – wurtzite – chalcopyrite – isocubanite – pyrite in worm-tube molds, the last remaining open conduits available through the now-silicified soot mounds. As the hydrothermal system waned, firstly clear silica spheroids precipitated into channelways, coating late euhedral sulfides, and then finally as buds, nucleating growths of exotic cylindrical transparent silica needles within worm-tube molds. The entire process must have been of very short duration given the ephemeral nature of the hydrothermal event, indicated by the small size attained by worm-tubes within these thinly crusted mounds. It is known from more recent studies of spreading events, concomitant active volcanism and associated hydrothermal activity at CoAxial segment, Juan de Fuca Ridge (Embley *et al.* 1995), that similar worm-tubes can grow to tens of cm in length and several cm in diameter over a few months, once the community is established, provided a supply of hydrogen sulfide is maintained in the warm vent fluids (Embley 1994, V. Tunnicliffe, pers. commun. 1995, and the authors' field observations). The presence of abundant sulfides in the Cleft mounds indicates that habitat conditions were ideal to support a juvenile biological community, but only for a very short period of time.

Undoubtedly the silica clusters and agglomerated sooty sulfides survived because of the shutdown of the transient hydrothermal system. Our sampling occurred within a few months of known megaplume events in the area, leaving little time for supergene diagenesis, involving warm seawater, to effect recrystallization.

Acknowledgements

We greatly appreciate the assistance of Peter Bélanger (Analytical Services), Gilles Lemieux (Photography) and Kathy Mooney (manuscript preparation), all of G.S.C. Peter Jones, Carleton University (SEM imagery and analysis) and Ingrid Kjarsgaard, G.S.C. (electron-microprobe analysis) contributed greatly to the study. Bob Embley (NOAA, Newport) and the crews of Atlantis II – ALVIN made things work at sea. We are most grateful for support for field programs and laboratory research provided by grants to MRP by the National Science Foundation (NSF–OCE 9100503) and the NOAA Vents Program. We thank the two referees for their useful comments and critiques.

References

Baker, E.T. (1994): A 6-year time series of hydrothermal plumes over the Cleft Segment of Juan de Fuca Ridge. *J. Geophys. Res.* **99**, 4889-4904.

Butterfield, D.A. & Massoth, G.J. (1994): Geochemistry of north Cleft Segment vent fluids: temporal changes in chlorinity and their possible relation to recent volcanism. *J. Geophys. Res.* **99**, 4951-4968.

Caye, R., Cervelle, B., Cesbron, F., Oudin, E., Picot, P. & Pillard, F. (1988): Isocubanite, a new definition of the cubic polymorph of cubanite $CuFe_2S_3$. *Mineral. Mag.* **52**, 509-514.

Davydov, M.P., Sudarikov, S.M. & Kolosov, O.V. (1998): Native metals and intermetal compounds in sediments and suspended matter of hydrothermal-active segments of the East Pacific Rise. *Lithol. Mineral. Res.* **33**, 14-25.

Delaney, J.R., Kelley, D.S., Lilley, M.D., Butterfield, D.A., Baross, J.A., Wilcock, W.S.D., Embley, R.W. & Summit, M. (1998): The quantum event of oceanic crustal accretion: impacts of diking at mid-ocean ridges. *Science* **281**, 222-230.

Embley, R.W., ed. (1994): N.O.A.A. Cruise Report. *N.O.A.A. Publ.* **131-16**.

_____ & Chadwick, W.W., Jr. (1994): Volcanic and hydrothermal processes associated with a recent phase of sea floor spreading at the northern Cleft Segment: Juan de Fuca Ridge. *J. Geophys. Res.* **99**, 4741-4760.

_____, _____, Jonasson, I.R., Butterfield, D.A. & Baker, E.T. (1995): Initial results of the rapid response to the 1993 CoAxial event: relationships between hydrothermal and volcanic processes. *Geophys. Res. Lett.* **22**, 143-146.

_____, Jonasson, I.R., Perfit, M.R., Franklin, J.M., Tivey, M.A., Malahoff, A., Smith, M.F. & Francis, T.J.G. (1988): Submersible investigation of an extinct hydrothermal system on the Galapagos Ridge: sulfide mounds, stockwork zone, and differentiated lavas. *Can. Mineral.* **26**, 517-539.

Flörke, O.W., Graetsch, H. & Jones, J.B. (1990): Hydrothermal deposits of cristobalite. *Neues Jahrb. Mineral., Monatsh.*, 81-95.

Halbach, P., Pracejus, B. & Märten, A. (1988): Geology and mineralogy of massive sulfide ores from the Central Okinawa Trough, Japan. *Econ. Geol.* **88**, 2210-2225.

HANNINGTON, M.D. (1993): The formation of atacamite during weathering of sulfides on the modern sea floor. *Can. Mineral.* **31**, 945-956.

_____ & JONASSON, I.R. (1992): Fe and Mn oxides at sea floor hydrothermal vents. *Catena Suppl.* **21**, 351-370.

_____ & SCOTT, S.D. (1988): Mineralogy and geochemistry of a hydrothermal silica–sulfide–sulfate spire in the caldera of Axial Seamount, Juan de Fuca Ridge. *Can. Mineral.* **26**, 603-625.

HAYMON, R.M. & KASTNER, M. (1986): Caminite: a new magnesium-hydroxide-sulfate-hydrate mineral found in a submarine hydrothermal deposit, East Pacific Rise, 21°N. *Am. Mineral.* **71**, 819- 825.

HERZIG, P.M., BECKER, K.P., STOFFERS, P., BÄCKER, H. & BLUM, N. (1988): Hydrothermal silica chimney fields in the Galapagos Spreading Center at 86°W. *Earth Planet. Sci. Lett.* **89**, 261-272.

IIZASA, K., KAWASAKI, K. MAEDA, K., MATSUMOTO, T., SAITO, N. & HIRAI, K. (1998): Hydrothermal sulfide-bearing Fe–Si oxyhydroxide deposits from the Coriolis Troughs, Vanuatu backarc, southwestern Pacific. *Marine Geol.* **145**, 1-21.

JUNIPER, S.K. & FOUQUET, Y. (1988): Filamentous iron–silica deposits from modern and ancient hydrothermal sites. *Can. Mineral.* **26**, 859-869.

KOSKI, R.A., JONASSON, I.R., KADKO, D.C., SMITH, V.K. & WONG, F.L. (1994): Compositions, growth mechanisms and temporal relations of hydrothermal sulfide–sulfate–silica chimneys at the northern Cleft Segment, Juan de Fuca Ridge. *J. Geophys. Res.* **99**, 4813-4832.

LOWELL, R.P. & GERMANOVICH, L.N. (1995): Dike injection and the formation of megaplumes at ocean ridges. *Science* **267**, 1804-1807.

NASDALA, L., WITZKE, T., ULLRICH, B. & BRETT, R. (1998): Gordaite, $[Zn_4Na(OH)_6(SO_4)Cl \cdot 6H_2O]$: second occurrence in the Juan de Fuca Ridge, and new data. *Am. Mineral.* **83**, 1111-1116.

ODP SHIPBOARD SCIENTIFIC PARTY (1995): TAG-2 area. *In* Proc. ODP, Initial Report **158** (S.E. Humphris, P.M. Herzig D.J. Miller *et al.*, eds.). Ocean Drilling Program, College Station, Texas (141-169).

OUDIN, E. (1983): Hydrothermal sulfide deposits of the East Pacific Rise (21°N). I. Descriptive mineralogy. *Marine Mining* **4**, 39-72.

_____, MARCHIG, V., ROSCH, H., LALOU, C. & BRICHET, E. (1990): Observation de CuS_2 à l'état naturel dans une cheminée hydrothermale du Pacifique Sud. *C.R. Acad. Sci. Paris* **310**, *sér.* **II**, 221-226.

PRACEJUS, P. & HALBACH, P. (1996): Do marine moulds influence Hg and Si precipitation in the hydrothermal JADE field (Okinawa Trough)? *Chem. Geol.* **130**, 87-99.

RONA, P.A., JACKSON, D.R., WEN, T., JONES, C., MITSUZAWA, K., BEMIS, K.G. & DWORSKI, J.G. (1997): Acoustic mapping of diffuse flow at a seafloor hydrothermal site: Monolith Vent, Juan de Fuca Ridge. *Geophys. Res. Lett.* **24**, 2351-2354.

STÜBEN, D., EDDINE TAIBI, N., MCMURTRY, G.M., SCHOLTEN, J. STOFFERS, P. & ZHANG, DEYU (1994): Growth history of a hydrothermal silica chimney from the Mariana backarc spreading center (southwest Pacific, 18°13'N). *Chem. Geol.* **113**, 273-296.

URABE, T. & KUSAKABE, M. (1990): Barite silica chimneys from the Sumisu Rift, Izu–Bonin arc: possible analog to hematitic chert associated with Kuroko deposits. *Earth Planet. Sci. Lett.* **100**, 283- 290.

VANKO, D.A., MILBY, B.J. & HEINZQUITH, S.W. (1991): Massive sulfides with fluid-inclusion-bearing quartz from a young seamount on the East Pacific Rise. *Can. Mineral.* **29**, 453-460.

Received July 13, 1998, revised manuscript accepted December 30, 1998.